January 18, 2006

Ken Zweibel
National Renewable Energy Laboratory
1617 Cole Boulevard
Golden, CO 80401

Re: NREL Subcontract #ADJ-1-30630-12

Dear Ken,

This report covers research conducted at the Institute of Energy Conversion (IEC) for the period November 9, 2005 to December 9, 2005, under the subject subcontract. The report highlights progress and results obtained under Task 2 ($CuInSe_2$-based Solar Cells).

TASK 2: $CuInSe_2$-BASED SOLAR CELLS

Thermal Modeling of Linear Source

In the previous report, two specific issues were discussed that must be resolved for a successful commercial-scale development of $CuInGaSe_2$ thin-film roll-to-roll deposition process, namely: (i) melt-temperature gradient and (ii) melt depletion. The first issue results in unequal vapor flux from the two nozzles affecting the film thickness uniformity, while the latter changes the temperature profile of the melt itself, making control of the melt-temperature difficult.

Experimental results were presented to show that the asymmetry in the heater-assembly (specifically, placement of both power leads on one end) caused the melt temperature gradient with the Lead Side (i.e. the power lead side) being cooler than the other (the Far Side). Hence, achieving acceptable film thickness uniformity is a design issue. On the other hand, melt depletion will occur irrespective of the source design used; therefore, its effect on the vapor flow rates should be rejected by a proper control strategy.

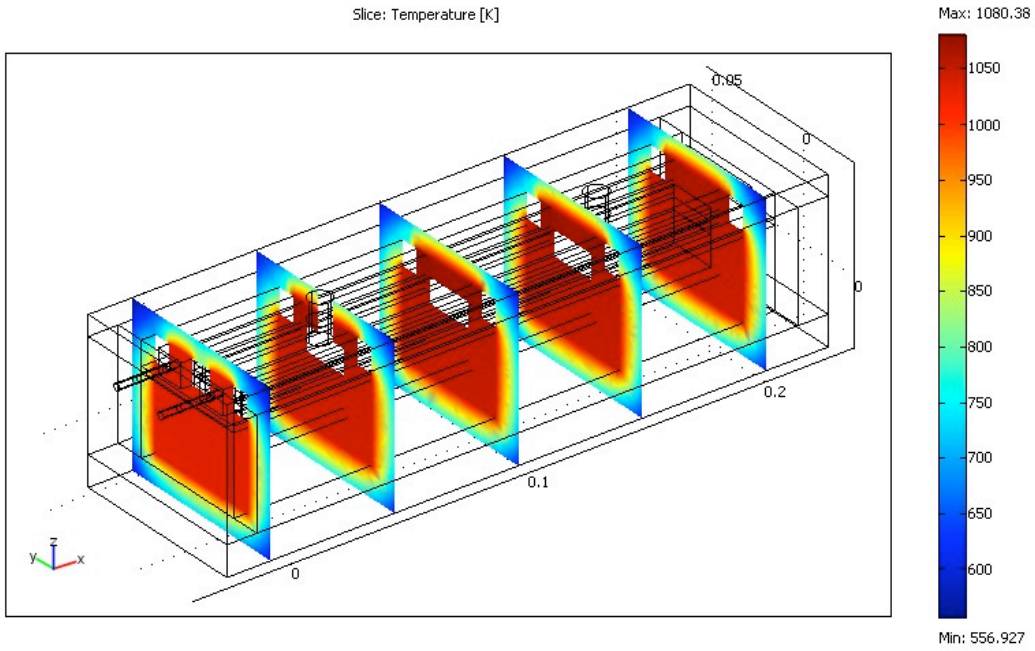

Figure 1. Source boat temperature profile: Asymmetric heater assembly.

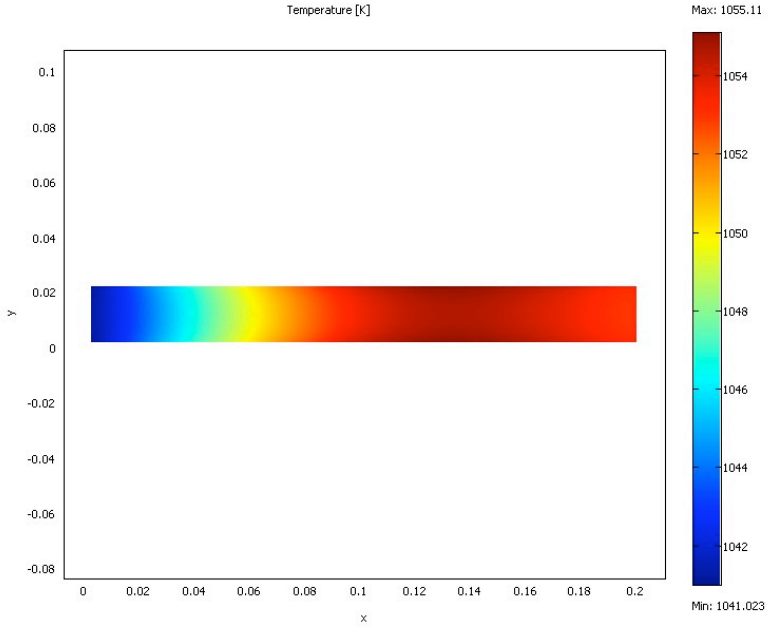

Figure 2. Copper melt-surface temperature profile: Asymmetric heater assembly.

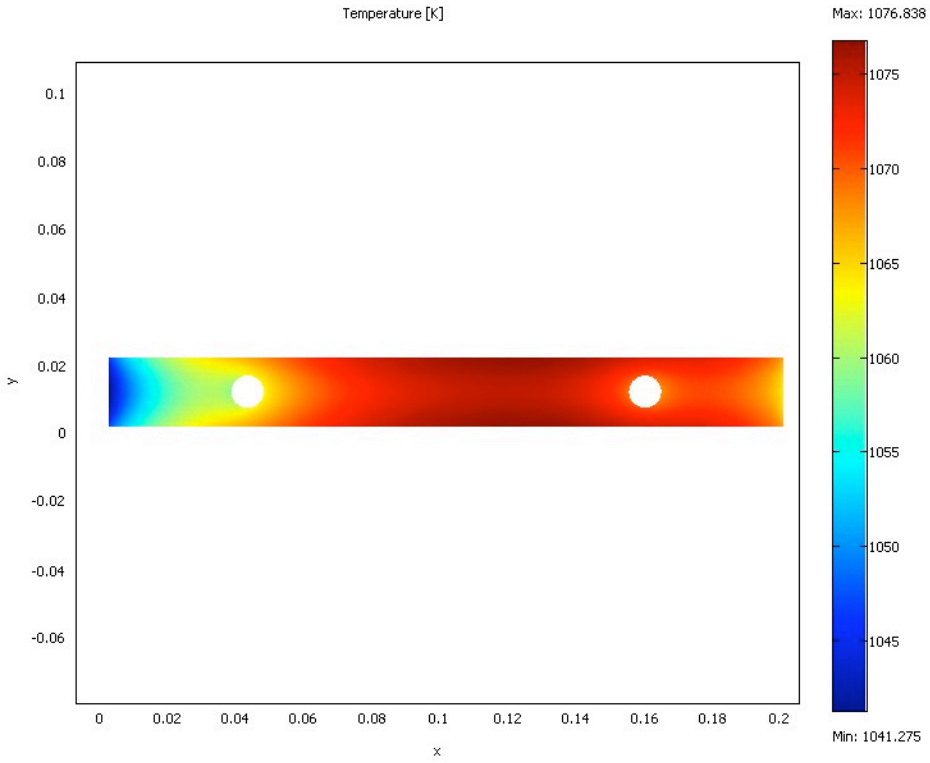

Figure 3. Lid temperature profile: Asymmetric heater assembly.

In this report, preliminary finite-element-based thermal modeling results for the linear source-boat (using COMSOL Multi-physics software package) are presented. In the face of difficulties in experimentally measuring the melt-temperature profile, thermal modeling is a good alternative to determine not only the melt surface temperature, but also the temperature profile of the whole boat. For this preliminary thermal analysis, rectangular geometry is assumed for all the source-boat components with the exception of the cylindrical nozzles and the current leads. The emissivity values of alumina insulation, copper melt, boron nitride and molybdenum current leads are assumed to be 0.3, 0.2, 0.3, and 0.2 respectively. The current in the heater is assumed to be 100 Amps. Figures 1, 2, and 3 show, respectively, the boat, melt and lid temperature profiles for the asymmetric heater-assembly. The temperature gradient from the Far side (hotter) to the Lead side (cooler) in each case is clearly observable. Figures 4, 5, and 6 show the similar results for the source with symmetric heater assembly. As expected, the melt temperature profile for this case is symmetric. The absolute temperatures are lower than the experimentally observed values, due to the emissivity and geometry assumptions used in the model.

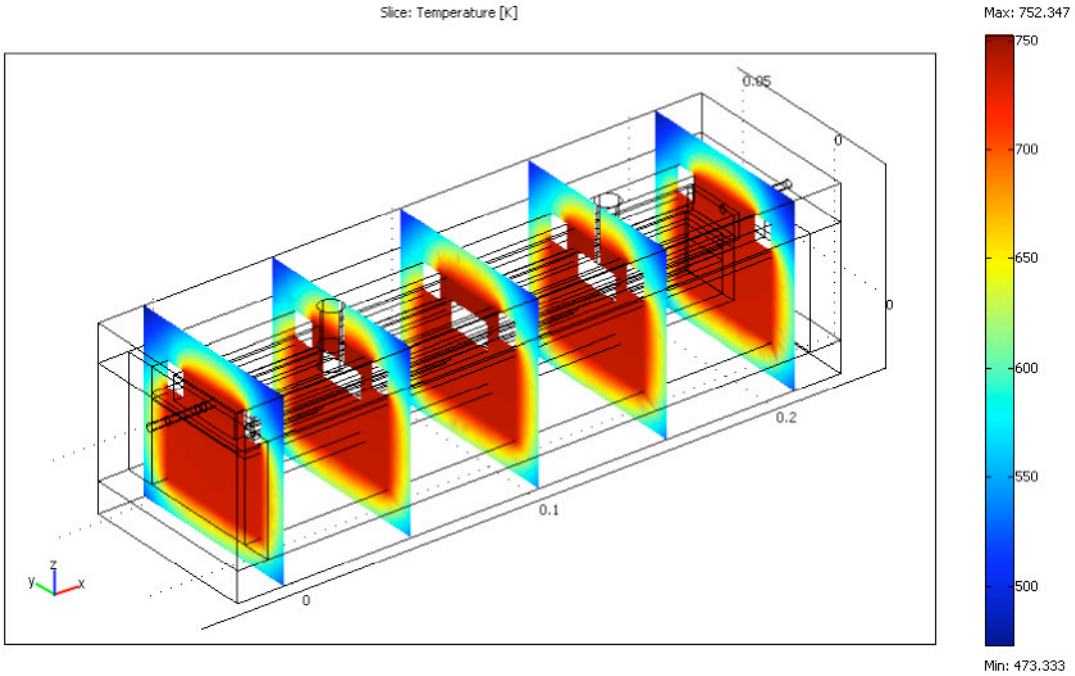

Figure 4. Source boat temperature profile: Symmetric heater assembly.

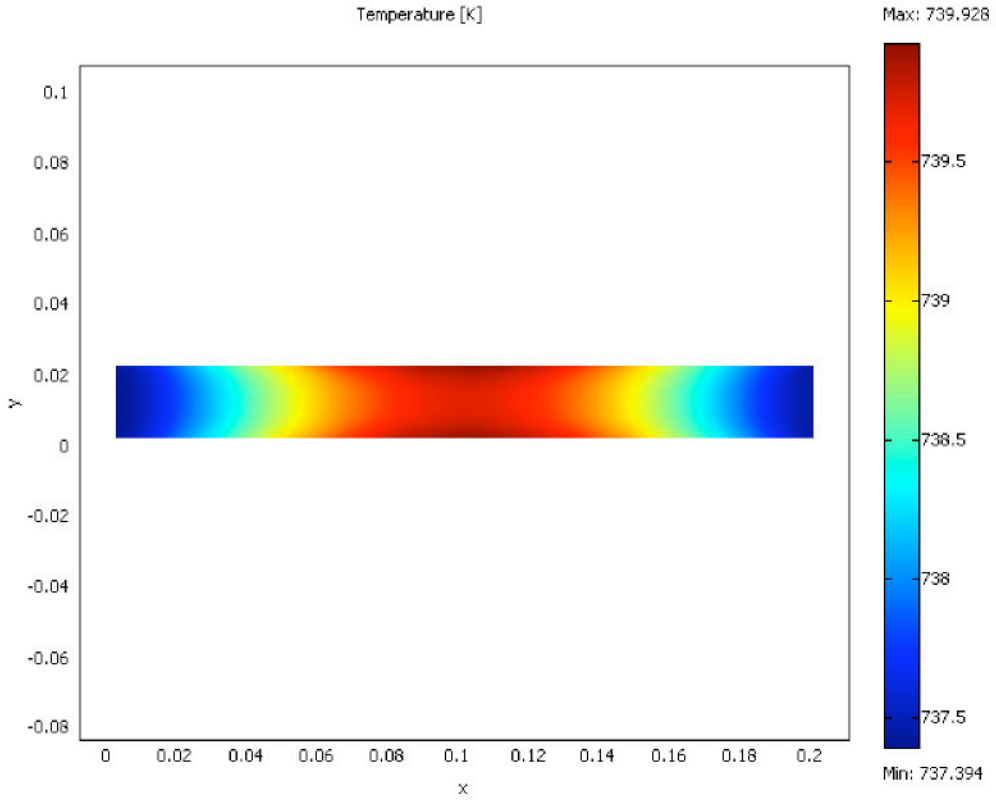

Figure 5. Copper melt-surface temperature profile: Symmetric heater assembly.

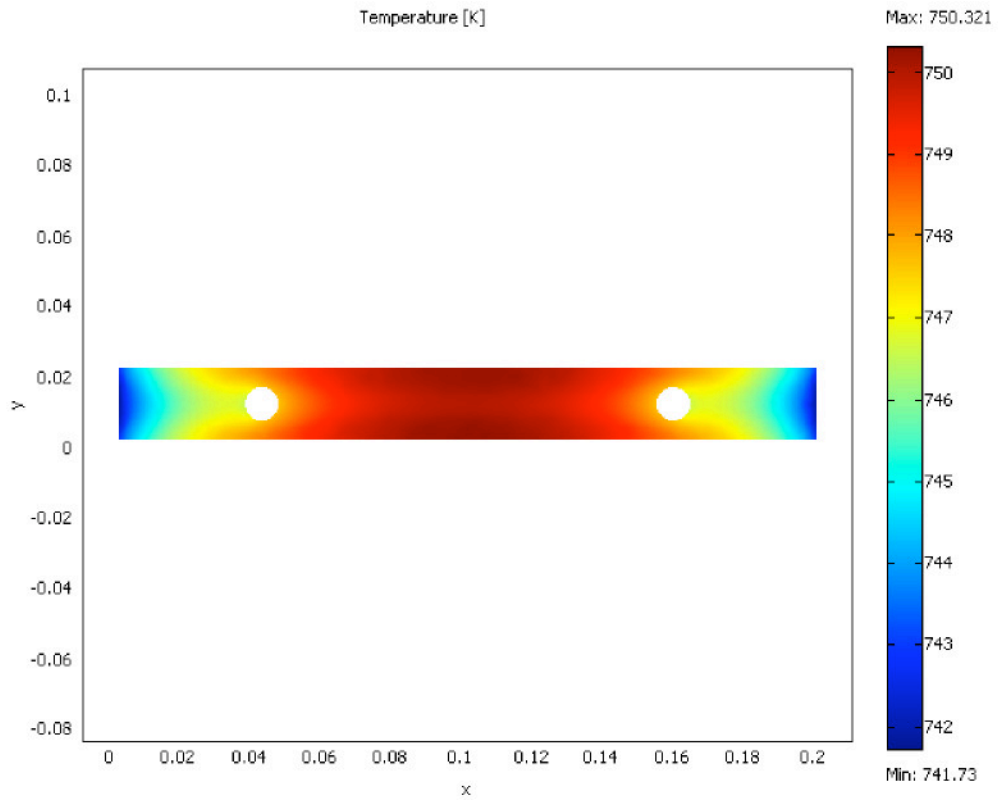

Figure 6. Lid temperature profile: Symmetric heater assembly.

Future modeling work will involve the use of more realistic surface emissivities, source geometry and transient response. Furthermore, it will be used to determine changes in the temperature profiles with melt depletion, which may then be used in the model predictive control strategy to achieve constant melt temperature for longer deposition times, where considerable reduction in melt level occurs.

Wide Bandgap Materials: $Cu(InAl)Se_2$

$Cu(InAl)Se_2$ films were deposited using the modified 3-stage process discussed in the 2005 Annual Report under this contract, and the process was used to characterize the properties of the $Cu(InAl)_2Se_{3.5}$ ordered vacancy phase (OVC) phase and its effect on the surface of the $Cu(InAl)Se_2$ layer in analogy to the $Cu(InGa)_2Se_{3.5}$ composition that typically forms on the surface of $Cu(InGa)Se_2$ films. The Cu-In-Al-Se films were deposited on a ~5nm thick sputtered Ga layer for better adhesion to the Mo back contact. First, films of the deposition rate and time were adjusted to give an expected composition ratio [Cu]/[In+Al] ≈ 0.5 corresponding to $Cu(InAl)_2Se_{3.5}$. The film compositions from EDS analyses are listed in Table I for two films deposited under the same condition except the 3rd stages, with only In-Al-Se flux, were grown at 450°C and 400°C respectively. The lower substrate temperature during the 3rd stage apparently results in a

lower concentration of Cu near the film surface. X-ray diffraction (not shown) of both films showed several diffraction peaks of the OVC phase.

Table I. Chemical composition of films determined by EDS analyses.

Sample	3rd stage	Cu (at%)	In (at%)	Al (at%)	Se (at%)	Composition formula
Expected composition [Cu]/[In+Al]~0.5 ($Cu(InAl)_2Se_{3.5}$)						
50616	450°C	12	25	8	55	$Cu(In_{0.75}Al_{0.25})_{2.9}Se_{4.8}$
50617	400°C	9	26	8	56	$Cu(In_{0.76}Al_{0.24})_{3.8}Se_{6.1}$
Expected composition [Cu]/[In+Al]~0.9 ($Cu(InAl)_{1.1}Se_{2.2}$)						
50614	~570°C	23	21	5	51	$Cu(In_{0.80},Al_{0.20})_{1.1}Se_{2.2}$
50621	450°C	22	21	6	50	$Cu(In_{0.77},Al_{0.23})_{1.2}Se_{2.3}$

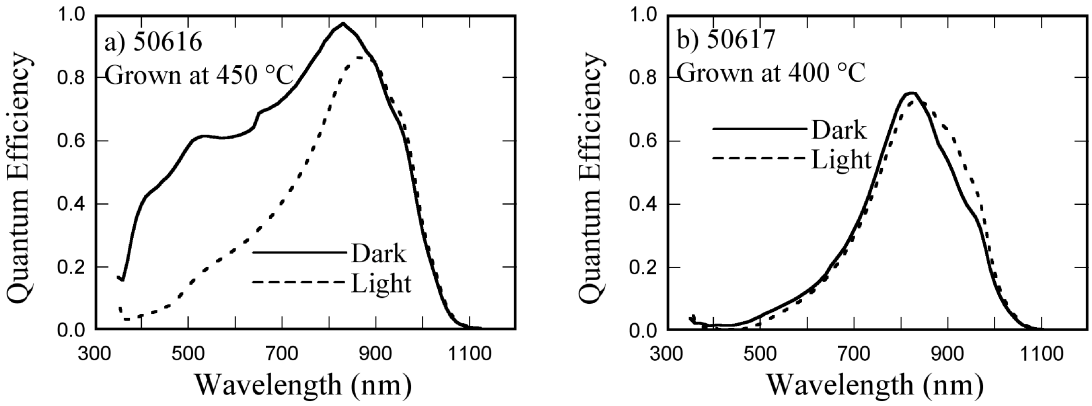

Figure 7. Internal Quantum Efficiency of samples (left) 50616 and (right) 50617.

Using those samples, devices with soda-lime glass/Mo/absorber/CdS/ZnO/ITO/Ni-Al structure were prepared. Figure 7 shows the quantum efficiency under illumination and in the dark. Under illumination, both devices show degraded response for wavelength below 850 nm. In the dark, on the other hand, an increase in the response below 850 nm is seen on sample (left) 50616 but not on sample (right) 50617.

Films (#50621) with [Cu]/[In+Al]~0.9 expected from the fluxes were also prepared. To form an OVC surface layer, based on the above results, the substrate temperature during the 3rd stage was dropped to 450°C from ~570°C. The film compositions of sample 50621 by EDS are listed in Table I along with the standard sample (#50614) with the 3rd stage deposited at 570°C. In Figure 8, grazing incidence x-ray diffraction profiles from sample 50621 are shown. The characteristic peaks from OVC are observed and their intensity relative to the chalcopyrite peaks does not change with incident angle from 2° to 4° suggesting that a relatively thin OVC surface layer was formed. The OVC peaks are

not observed in the control film #50614 with high temperature in the 3rd stage or with $Cu(InAl)Se_2$ films deposited using a single layer deposition.

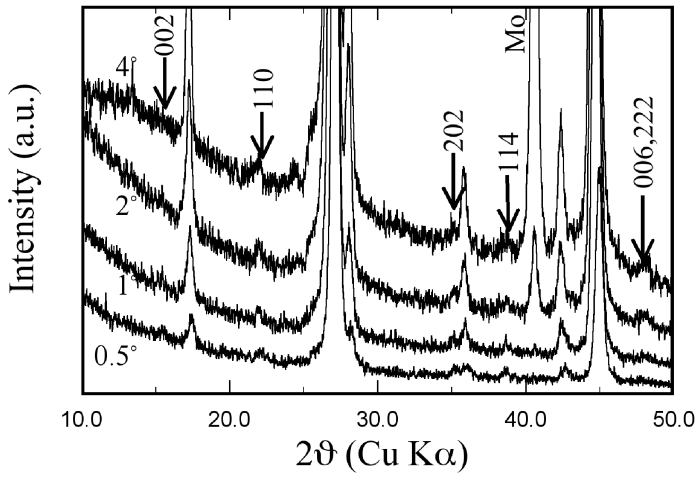

Figure 8. GIXRD profiles of sample 50621 with peaks indexed to the $Cu(InAl)_2Se_{3.5}$ phase. Grazing angles are 0.5°, 1°, 2° and 4° from the bottom to top.

Table II lists solar cell properties for sample #50621 and standard #50614 and they have similar QE curves so there is no apparent difference in cells with the surface OVC layer.

Table II. $Cu(InAl)Se_2$ solar cell J-V parameters.

Sample	Eff. (%)	V_{oc} (V)	J_{sc} (mA/cm^2)	FF (%)
50614	11.9	0.637	28.8	64.9
50621	12.0	0.628	29.2	65.5

$Cu(InGa)(SeS)_2$ Formation by H_2Se/H_2S Reaction

Recent studies of the selenization/sulfurization of Cu-Ga-In precursors shown in the 2005 Annual Report under this contract have yielded some results not previously observed by Marudachalam et. al.[1] Specifically, the new data have indicated the presence of a $Cu_9(In_{1-x}Ga_x)_4$ intermetallic after annealing at 450 ºC (the baseline selenization temperature for Ga-containing precursors) and a robust Cu_9Ga_4 at the back of the film after reaction in H_2Se. Experiments were done to determine if these observations are related to a change in precursor structure – Marudachalam used 3-layer precursors sputtered from elemental Cu, Ga, and In targets, while the recent work has used 2-layer precursors sputtered from a $Cu_{0.8}Ga_{0.2}$ alloy target and an elemental In target.

Sputter deposition was used to prepare two types of precursors: 3-layer Cu/Ga/In and 2-layer $Cu_{0.8}Ga_{0.2}$/In precursors. Both precursor types had a target composition of Cu/(Ga+In) = 0.9 and Ga/(Ga+In) = 0.22 and their thicknesses corresponded to a 2 μm $Cu(InGa)Se_2$ film. One of each precursor type was annealed side-by-side in a quartz tube reactor for either 60 min at 250ºC, or 10 min at 450ºC. The anneals were performed in flowing Ar with no O_2 or hydride gases present. The lower temperature anneal was that performed by Marudachalam, while the higher temperature anneal was used in recent work.

SEM micrographs of the as-deposited 3-layer and 2-layer precursors are shown in Figure 9. There is no significant difference in morphology. The phases observed by XRD in the as-deposited films are shown in Table III. The only difference between the two precursor structures is the observation of $CuGa_2$ in the Cu/Ga/In precursor. This is likely explained by the progression from Cu, to Cu-rich Cu_3Ga alloy, to Ga-rich $CuGa_2$ alloy, to Ga at the Cu/Ga interface during Ga sputtering. $CuGa_2$ is not observed in the 2-layer precursor because a Ga-rich phase never has the opportunity to form with the Ga constantly surrounded by a Cu-rich alloy phase. The morphology of the precursors did not change during annealing.

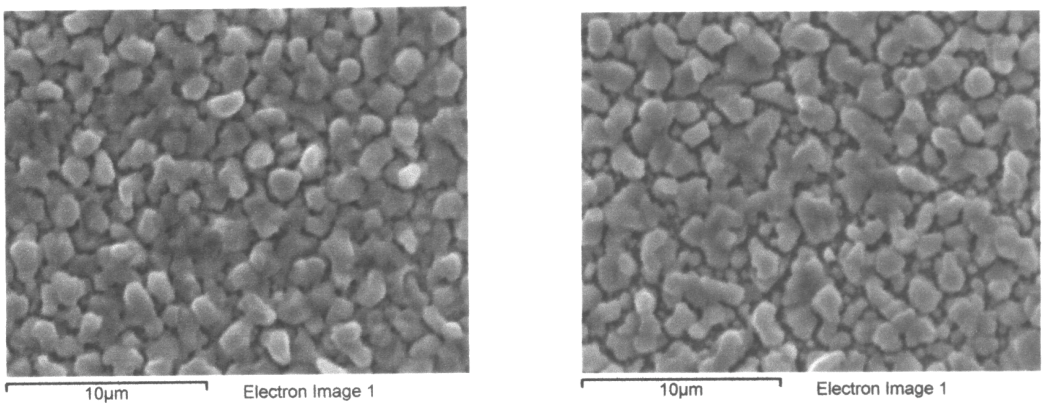

Figure 9. Morphology comparison of Cu/Ga/In (left) and $Cu_{0.8}Ga_{0.2}$/In (right) precursors.

Table III. Phases observed by XRD in as-sputtered precursors.

Precursor	Phases observed
Cu/Ga/In	In, CuIn, $CuGa_2$, Cu_3Ga, Cu
$Cu_{0.8}Ga_{0.2}$/In	In, CuIn, Cu_3Ga, Cu

Figure 10 compares the XRD spectra of the precursors after annealing at 250ºC. In each case, the spectra contain elemental In and $Cu_9(In_{1-x}Ga_x)_4$ intermetallic phases (denoted γ_1) whose compositions are estimated by Vegard's law from the Cu_9Ga_4 – Cu_9In_4 endpoints. The $Cu_{0.8}Ga_{0.2}$/In precursor exhibited the same $Cu_9(In_{0.64}Ga_{0.36})_4$ phase as found in precursors heat treated at 450ºC. The Cu/Ga/In precursor exhibited two compositions of the $Cu_9(In_{1-x}Ga_x)_4$ phases, as observed by Marudachalam, with compositions $Cu_9(In_{0.74}Ga_{0.26})_4$ and $Cu_9(In_{0.21}Ga_{0.79})_4$. The Ga-rich intermetallic is apparently present in minute quantities, so only its strongest peak at 43.7º is observed. There are differences observed in the In orientation, but this is likely irrelevant to the intermetallic phases observed.

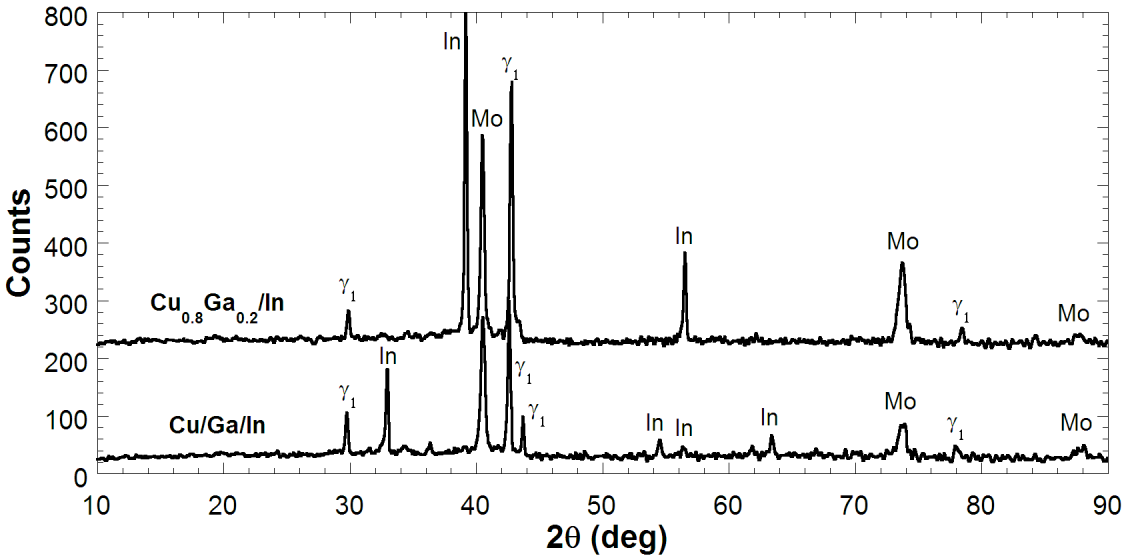

Figure 10. XRD spectra of precursors annealed for 60 min at 250 ºC. γ_1 is the intermetallic alloy $Cu_9(In_{1-x}Ga_x)_4$.

Figure 11 compares the XRD spectra of the precursors after annealing at 450 ºC for 10 min. In this case, the films show the identical $Cu_9(In_{0.64}Ga_{0.36})_4$ phase that was observed in the 250ºC $Cu_{0.8}Ga_{0.2}$/In precursor. Again, there are variations in indium orientation, which bear no significance to the intermetallic phase behavior.

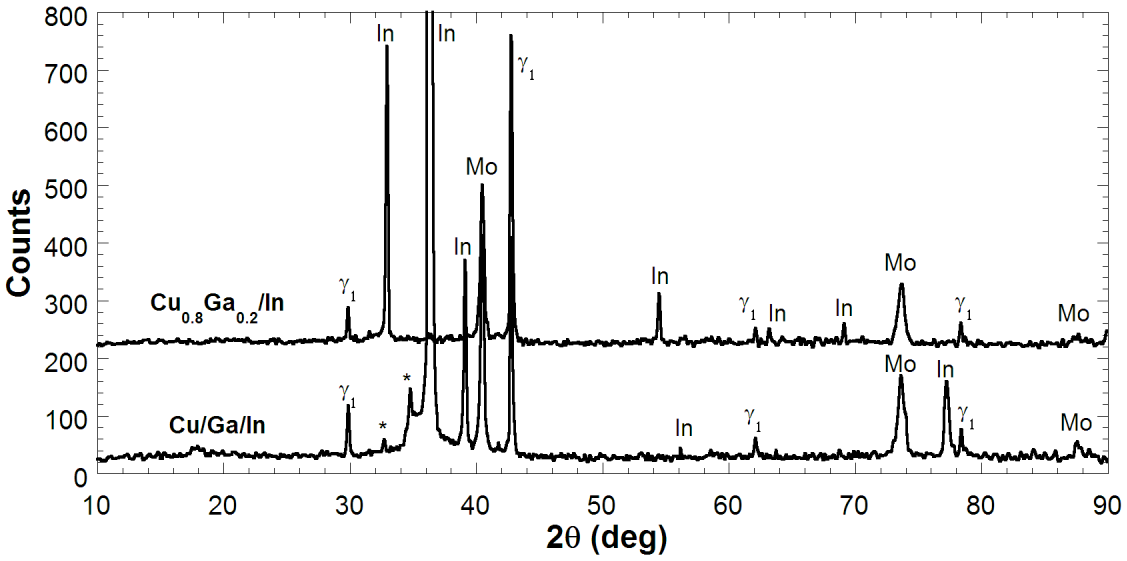

Figure 11. XRD spectra of precursors annealed for 10 min at 450ºC. Asterisks denote CuK_β and WL_α artifacts from In 002 peak at 36.4º.

The results demonstrate that the two precursor structures exhibit no difference in phase behavior at the typical reaction temperature of 450 ºC. Results of the different precursor films reacted in H_2Se will be presented in the next report.

Fundamental Materials and Interface Characterization

Further experiments have been done to characterize the effects of an aqueous Br-etch[2] as a tool to study solar cells with thin $Cu(InGa)Se_2$ absorber layers. The thickness is controlled by the time of the Br-etch which is followed by a KCN etch to prepare the surface for devices. After etching, the thickness is determined from the optical interference fringes, using the refractive index determined by spectroscopic ellipsometry.[3]

Device results with different etch times and thicknesses $1.6 > d > 0.4$ μm are shown in Table IV and are compared to the as-deposited film. A cell with 12.7% efficiency was achieved with a 0.55 μm absorber layer. All the etched films had lower V_{oc}, as in previous experiments, but there was no consistent decrease was constant for $d > 0.5$ μm. The FF remained ≥ 74% even for d = 0.43 μm. J_{sc} decreased for d < 1 μm as expected due to incomplete optical absorption.[4] QE curves for these cells are shown in Figure 12 and show a loss in the long wavelength end of the spectra. These cells have some variation in the band edge, apparently due to variations in the relative Ga content.

In addition to studying the effect of absorber thickness on devices, one of the objectives of reducing thickness is to gain better access to the back contact for structural

characterization using XRD. Preliminary measurements with an 0.5 µm Cu(InGa)Se_2 layer did not reveal any diffraction peaks due to $MoSe_2$ expected to form at the MO/Cu(InGa)Se_2 interface. Further characterization, including current-voltage-temperature measurements is being completed. In addition, layers with more uniform composition are being grown simultaneously on Mo and transparent substrates (glass and ITO-coated glass) to enable additional optical measurements.

Table IV. Cu(InGa)Se_2 thickness and device J-V parameters as a function of Br-etch time of the Cu(InGa)Se_2 absorber layer.

etch time (min)	Cu(InGa)Se_2 *d* (µm)	η (%)	V_{oc} (V)	J_{sc} (mA/cm^2)	FF (%)
as-dep	1.7	14.8	0.623	31.5	75.2
1	1.57	13.9	0.606	30.5	75.3
5	0.84	11.2	0.580	26.6	72.9
7	0.55	12.7	0.617	28.0	73.7
9	0.43	9.5	0.563	22.6	74.4

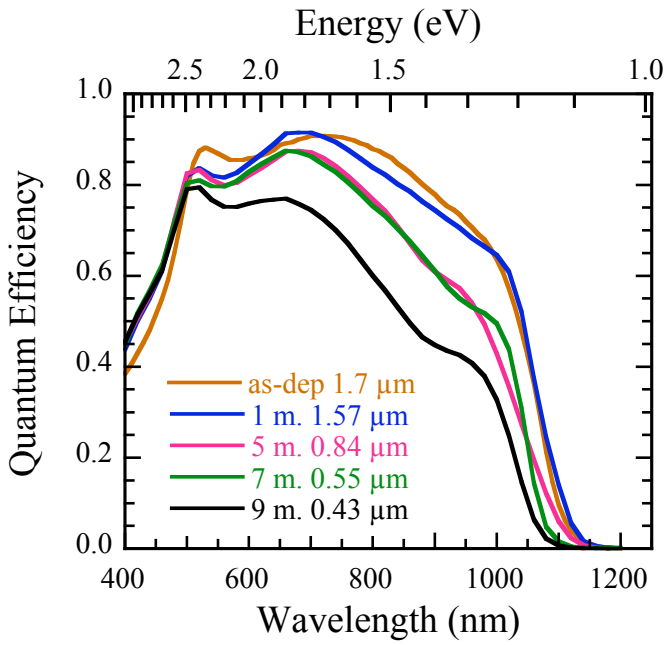

Figure 12. QE with etched Cu(InGa)Se_2 with thicknesses 1.6 >d >0.4 µm. Measurements were done under white light bias at 0V.

Collaboration

IEC has continued collaboration with EPV on alternative back contacts. A paper partly on this work was presented at the 2005 AVS International Symposium in Boston "TiN and TiO_2:Nb Thin Film Preparation Using Hollow Cathode Sputtering with Application to Solar Cells" by S.Y. Guo, W.N. Shafarman, and A.E. Delahoy.

References

1. M. Marudachalam, H. Hichri, R.Klenk, R.W. Birkmire, W.N. Shafarman and J.M. Schultz, Appl. Phys. Lett. **67**, 3978 (1995).
2. R.W. Birkmire, B.E. McCandless, Appl. Phys. Lett. **53**, 140 (1988).
3. R. Swanepoel, J. Phys. E **16**, 1214 (1983).
4. O. Lundberg, M. Bodegard, J. Malmstrom L. Stolt, Prog. Photovolt **11**, 77 (2003).

Best regards,

Robert W. Birkmire
Director

RWB/bj
cc: Gerri Hobbs, UD Research Office
Carolyn Lopez, NREL
Paula Newton
Erten Eser
William N. Shafarman